Iranian Journal of Materials Science and Engineering, Vol. 18, Number 2, June 2021
RESEARCH PAPER

Influence of Heat Treatment on the AA6061 and AA6063 Aluminum Alloys Behavior at Elevated Deformation Temperature

Masumeh Mohammadi, Hamidreza Rezaei Ashtiani*

* *hr_rezaei@arakut.ac.ir; hrr.Ashtiani@gmail.com;*
School of Mechanical Engineering, Arak University of Technology, Arak, Iran

Received: July 2020 **Revised: November 2020** **Accepted: December 2020**
DOI: 10.22068/ijmse.1890

Abstract: *The hot deformation behavior of the heat-treated AA6061 and AA 6063 aluminum alloys by T6-1, T6-2 artificial aging treatment, and O annealing treatment were studied by compression testing over a temperature range of 350–550°C and strain rates of 0.005-0.1 s^{-1}. It was observed that the flow stresses of the studied aluminum alloys treated by the T6-1 and T6-2 heat treatments were significantly higher than those of the O annealing treatment. Moreover, the stress-strain curves of the heat-treated alloys by the T6-1, T6-2, and O heat treatments demonstrated significant softening during deformation at the lowest strain rate under any of the deformation conditions. For several strains, the activation energy of hot deformation was specified and obtained to vary significantly with strain for the heat-treated alloys by the T6-1 and T6-2 treatments. The stress-strain data calculated from a linear equation, with strain-dependent parameters, shows a great fit with the experimental data for the heat-treated aluminum alloys.*

Keywords: *Hot deformation; AA6061; AA6063; Flow stress; Heat treatment; Aging; Annealing.*

1. INTRODUCTION

Over the years, the 6xxx series aluminum alloys with precipitation-hardening properties have had an extensive applications in various industries such as aerospace, automotive, and marine due to their superior mechanical properties such as high strength-weight ratio, low density, and excellent weldability [1, 2]. For instance, the aluminum alloys usage for typical automobile body parts can offer a mass reduction of up to 50% compared to steel. Nevertheless, as a consequence of their weak formability at room temperature, their applications have been restricted. To overcome this problem, the process of forming at elevated temperatures has been established due to their significant formability under this condition [3]. The chemical composition, heat treatment parameters, and production conditions have a significant effect on the formability of aluminum alloy. This implies that the properties of various aluminum alloys can be manipulated through special heat treatment processes. Accordingly, the heat treatment can be carried out either through solution heating or artificial aging. In the solution heating process, the group 6xxx of aluminum alloys are heated to a temperature range of 400-500ºC, before water quenching at ambient temperature, while artificial aging or age hardening is performed at a temperature range of about 140 to 180°C [4-6]. The AA6061 and AA6063 are composed of silicon and magnesium as their main alloying elements. The alloys have an acceptable welded ability and exhibit acceptable mechanical properties. Therefore, they are known as two of the most familiar aluminum alloys having widespread general-purpose applications [7]. In comparison to the aluminum alloy, the thermal softening causes to readjust the strain hardening and strain rate hardening of steel alloy arising from the adiabatic temperature rise during dynamic deformation [1]. The isothermal holding of the steel at a temperature of 850°C after the end of deformation makes further microstructure refinement through meta dynamic and static recrystallization [8].

About 80% of all metal products that consist of aluminum alloys experience hot forming in some steps of their processing history [9]. The hot deformation processes are considered as key and significant steps in the fabrication of engineering parts that need not only dimensional accuracy but also proper microstructural and mechanical properties. Therefore, verification and prediction of material response during hot deformation are very significant and considerable. The Arrhenius-type and Johnson-Cook (J-C) models are two conventional in phenomenological constitutive models [10-12]. The J-C model can forecast the deformation behavior of nonferrous materials at

[DOI: 10.22068/ijmse.1890]

elevated temperatures [13-15]. Many constitutive equations developed in predicting and estimating the thermomechanical behavior of aluminum alloys use the Zener–Holloman parameter which considers the effect of temperature and strain rate. In this regard, Rezaei Ashtiani et al have reported thermomechanical behavior of the AA1070, AA2030, and AlCuMgPb, AA7022-T6 aluminum alloys using the Zener-Holloman parameter in the developed constitutive equation to predict and calculate the hot flow stress of the mentioned alloys [9, 16-18]. The effects of deformation temperature, strain rate, strain are considered in the Arrhenius-type model to predict the flow stress of materials. Li et al. [19] investigated the Arrhenius-type model of the hot flow behavior of AA6082 aluminum alloy. Liu et al. [20] characterized the flow behavior of Al-Mg-Si-Mn-Cr alloy at elevated temperature and predicted by the phenomenological and physical-based models. Mostafaei et al. [21] proposed that the DRV occurred during hot compression of Al-6Mg and provided the Arrhenius model. Nayak et al. [22] compared the Arrhenius, strain-compensated Arrhenius, J-C, and modified J-C models of Al-SiC composite in a broad range of strain rate and temperatures. The hot deformation performance of the material is commonly simulated by two famous tests including hot tensile and hot compression, due to their similarity to hot forging, extrusion, and rolling processes [16, 23-25]. Hot-working comprises several aspects such as forging, rolling, and extrusion [26].

Material flow performance in hot forming processes have complexity usually affected by metallurgical phenomena like dynamic recovery (DRV), work hardening, and dynamic recrystallization (DRX) [9, 27]. It has been well confirmed that the microstructure restoration of alloys with high stacking fault energy (SFE) like aluminum alloys is accomplished through a variety of mechanisms such as DRV and DRX. This has been investigated by numerous researchers in the case of various aluminum alloys such as AA6061, AA6063, and AA5052 alloys. The results indicate the dominant effects of these mechanisms on the restoration of the microstructure of the aforementioned alloys [28-30].

Investigations reveal that the peak stress value decreases with the increase in deformation temperatures and decrease strain rates. Whereas the true strain rate held fixed, the dynamic softening effect causing the decrease of stress was clearer at higher deformation temperatures. At a specified temperature, a higher strain rate leads to higher peak stress [31]. Together with DR, coarsening and dynamic precipitation give rise to flow stress softening when deformation temperature is low, while dynamic recovery and dynamic recrystallization are the most important reasons for the flow stress softening when deformation temperature is higher for the alloys after solution treatment [32, 33]. The uni-axial compression tests at a temperature range of 25-400◦C and strain rates of 0.003, 0.03, and 0.3 s^{-1} had been utilized to study the flow stress behavior of AA2017–10 vol% SiCp. The results show that the dynamic strain aging takes place in AA2017 composite and consequently causes negative strain rate sensitivity in warm deformation [34].

The precipitations and or second phase particles have different and significant effect on the recrystallization and softening or hardening behavior of metallic materials depending on their sizes and distribution of these particles [35-38]. Fine second phase particles can suspend recrystallization by inflicting drag pressure on the grain boundary migration which is known as the Zener pinning effect [39]. Zener pinning plays a significant role in retarding primary recrystallization. Coarse particles consist of some intermetallic phases formed during casting are preferred sites for particle stimulated nucleation (PSN) and accelerate recrystallization [40]. Eivani et al. developed an analytical model of recrystallization combining grain boundary (GB) and PSN in hot deformed Al–4.5Zn–1Mg aluminum alloy. This research showed that the critical size of particles to act as PSN sites is strongly dependent on the strain rate and deformation temperature, as the critical particle size decreases particularly with increasing strain rate (bigger than 5 s^{-1}) at a specific deformation temperature. Whereas the critical particle size increases significantly with increasing deformation temperature at a given strain rate, and also the number of nuclei decreases with increasing deformation temperature and decreasing strain rate [41].

Although the impact of the hot deformation on the precipitation kinetics during the subsequent artificial aging has been studied, there are few works published on the influence of the dynamic precipitation on the hot deformation behavior of

[DOI: 10.22068/ijmse.1890]

aluminum alloys. Moreover, there is less published research on the hot deformation behavior for AA6082 aluminum alloy under heat treatment alloys [42]. Also, the constitutive equations in most published works usually include several constants that are calculated for the peak stress value only, as they assume that the flow stress is not dependent on the strain. For some aluminum alloys, work softening occurs in the course of hot deformation [34].

This research paper intends to investigate the influence of heat treatment (age hardening of T6-1, T6-2, and annealing of O) on the hot deformation behavior of AA6061 and AA6063 aluminum alloys at different temperatures and strain rates. In addition, the effect of dissimilar factors including the annealing and aging heat treatments, the deformation temperatures, and the strain rate on the hot deformation features of AA6061 and AA6063 (Al-Si-Mg) aluminum alloys will be inspected via isothermal hot compression tests.

2. MATERIALS AND EXPERIMENTAL METHODS

The chemical compositions of the AA6061 and AA6063 aluminum alloys extruded rod are shown in Table 1 and Table 2, respectively.

Table 1. Chemical composition (wt.%) of the AA6061 aluminum alloy.

Element	Al	Cr	Cu	Fe	Mg	Mn	Si	Ti	Zn
wt.%	97.5	0.15	0.23	0.24	1.08	0.03	0.62	0.01	0.05

Table 2. Chemical composition (wt.%) of the AA6063 aluminum alloy.

Element	Al	Cr	Cu	Fe	Mg	Mn	Si	Ti	Zn
wt.%	96	0.03	0.04	0.21	0.71	0.04	0.46	0.02	0.01

A series of cylindrical samples were machined from the extruded bars in the sizes of 14 mm and 21 mm in diameter and height, respectively. As it is clear in Figure 1, the extruded samples were heated in a furnace to the solution temperature of 520°C held for 2 hours, and subsequently quenched into water. Quenching to room temperature from the solution temperature produces the supersaturated solid solution phase (SSSP).

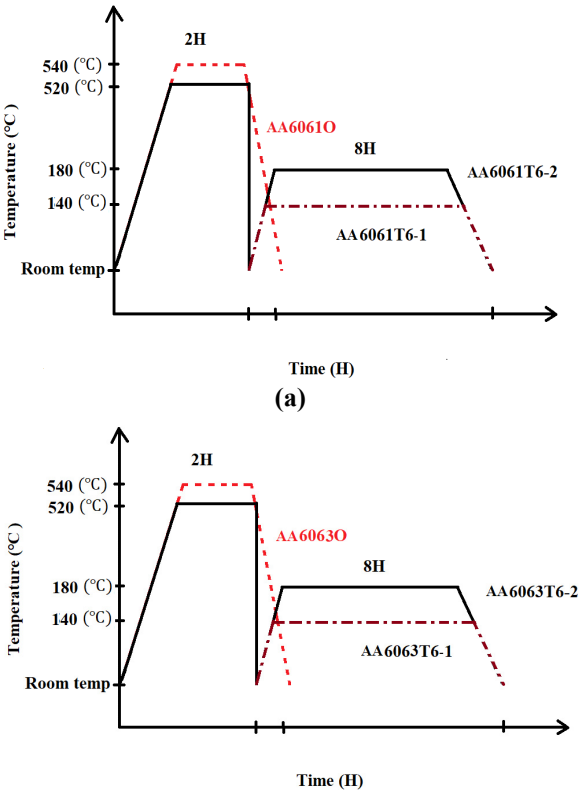

Fig. 1. Schematic of artificial aging heat treatment (T6-1 and T6-2 treatment) and annealing heat treatment (O treatment) for (a) AA6061 and (b) AA6063 aluminum alloys.

Then the specimens were subjected to artificial aging at temperatures 140°C and 180°C up to 8 h for AA6061 T61 or AA6063 T61 and AA6061 T62 or AA6063 T62, respectively. Slow cooling is avoided after SSSP to prevent the separation of equilibrium precipitate from solid solution. At elevated temperature, the aging (artificial aging) produces the non-equilibrium metastable or transition phases such as Guinier-Preston (GP) zones and hexagonal β″ and β′ (Mg_2Si) which is coherent to the matrix and strengthening occurs. These β″ and β′ (Mg_2Si) are coherent, unlike incoherent equilibrium fcc-β (Mg_2Si) and they are the sources of precipitation hardening or age hardening of AA6061 and AA6063 aluminum alloys. The age-hardenable precipitation formation sequence in AA6061 and AA6063 aluminum alloys from SSSP to GP then β″ and β′, and finally, β phase or Mg_2Si as these were

[DOI: 10.22068/ijmse.1890]

reported by other researchers [43-45].
The annealed AA6061 and AA6063 (AA6061 O and AA6063 O) aluminum alloys are heat treated to solution treatment at 520°C for 2 hours, then cooled in the air to room temperature (Figure 1). The microstructures of initial and deformed specimens were examined by an optical microscope (OM). To examine the region of the metallographic study, the optical micrographs were taken from the center of the specimens. The samples were prepared for OM by mechanical polishing and etching with a reagent that was used for AA6061 and AA6063 is 25% HNO3, 25% HCl, 50% warmed distilled water at different temperature. The presence of friction changes the test conditions from uniaxial deformation to 3-D deformation and consequently has a negative effect on the data accuracy, so the friction effect on the experimental data should be considered for predicting the accurate flow stress. The corrected flow stress was obtained in this study, as it was presented in Ref. [18]. Besides, to minimize the friction effect on flow stress, a very thin mica film was placed between fixture and specimens [2].
The optical micrograph of AA6061T6-2 and AA6061O, AA6063-T6-2, and AA6063-O aluminum alloys specimens before hot forming have been shown in Figure 2 (a & b), and Figure 3 (a & b), respectively. Also, the Optical micrograph of precipitates in A6061 O and AA6061 T6-2 aluminum alloy have been shown in Figure 4 (a & b), respectively. The particle stimulated nucleation (PSN) sometimes is known as one of the mechanisms in deformed microstructures of aluminum alloys [46]. As it is clear in Figure 4(b), the precipitations and secondary phase particles of Mg_2Si were found in the microstructure of AA6061-T62.

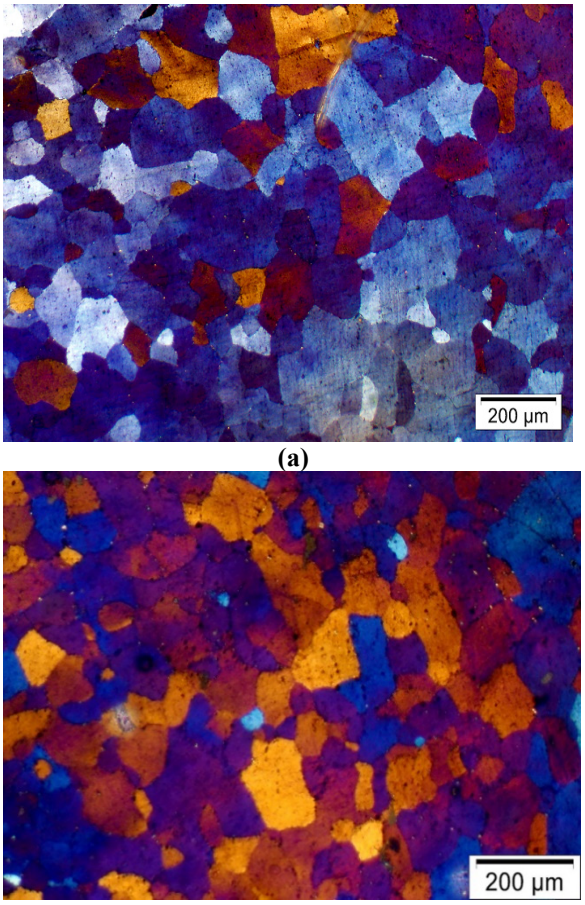

Fig. 2. Optical micrograph of the initial microstructure of (a) AA6061 O and (b) AA6061 T6-2 aluminum alloys.

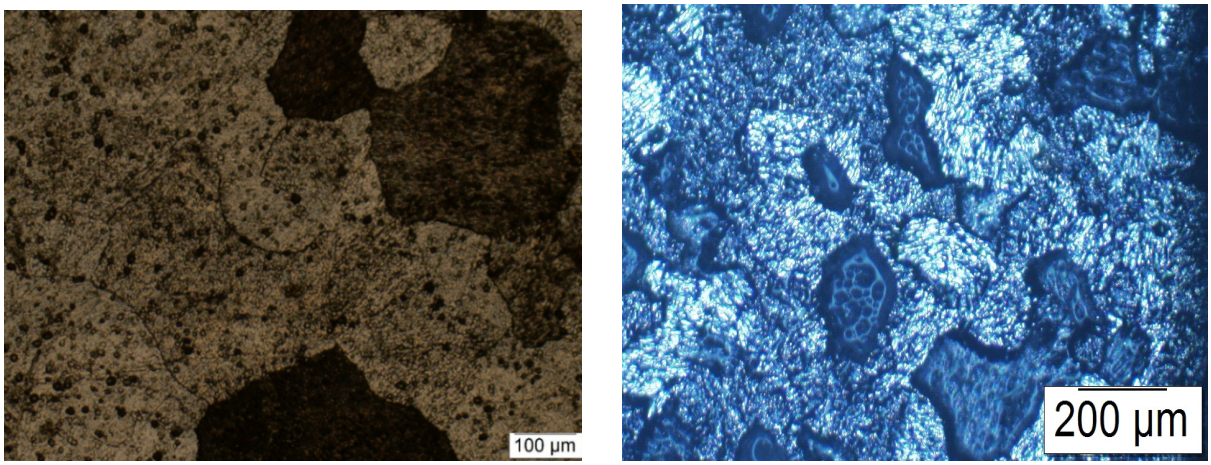

Fig. 3. Optical micrograph of (a) AA6063-O and (b) AA6063T6-2 aluminum alloys.

[DOI: 10.22068/ijmse.1890]

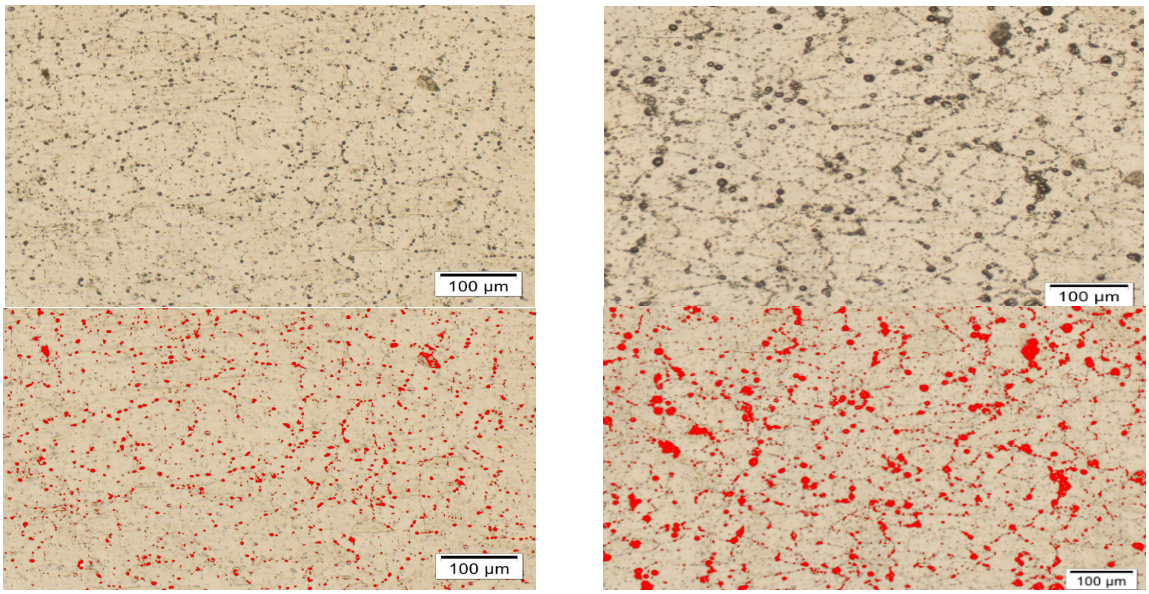

(a) (b)

Fig. 4. Optical microscope images of precipitates in (a) AA6061 O and (b) AA6061 T6-2 aluminum alloy.

To determine the true stress-strain behavior of these aluminum alloys, uniaxial one-hit hot compression tests were performed using a servo-controlled electronic universal testing machine equipped with an electrical resistance furnace. True stress values were recorded using a high accuracy load cell with the ability to measure load forces down to 1 kg. True strain values were computed from displacement data reported by the computer. Thin pieces of mica sheet were laid between punch and specimens as a lubricant material to reduce the friction throughout hot deformation. All the specimens were heated inside the closed chamber at a uniform heating rate of 100 /min to the specified temperature and soaked for 4 min to ensure homogenous temperature distribution throughout specimens.

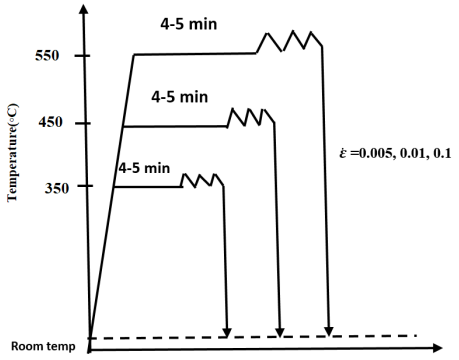

Fig. 5. Thermo-mechanical schematic used to compress samples that represent processing conditions.

Compression tests were carried out uniaxially up to the true strain of 0.8 and at different temperatures of 350, 450, and 550°C and strain rates of 0.005 s^{-1}, 0.01 s^{-1}, and 0.1 s^{-1}. Compressed samples were quenched in cool water immediately after compression to retain the deformed microstructure. Figure 5 illustrates the test timetable conditions for all heat-treated aluminum alloys. Force–displacement data had been converted to true stress–true plastic strain curves and then corrected for friction by barreling effect, after applying test condition on specimens.

3. RESULTS AND DISCUSSION

3.1. True stress-true strain curve of AA6061 T6-2 and AA6063 T6-2

At a homologous temperature above 0.6-0.7 Tm (Tm=melting temperature) plastic deformation is effectively affected by thermally activated processes therefore the materials flow behavior becomes dependent on strain rate and temperature [34].

The experimental investigations indicate the effects of deformation temperature and strain rate on the flow stress are major for all processing conditions. The true stress versus true strain curves obtained during the hot compression test under various strain rates and temperatures for

[DOI: 10.22068/ijmse.1890]

AA6061 T62 and AA6063 T62 have been presented in Figure 6 and Figure 7, respectively. As it is clear from these figures and as other samples of AA6061 O, T61 and AA6063 O, T61 the increase of strain rate and the decrease of deformation temperature can increase flow stress. Also, the effects of strain on the flow stress are obvious. A similar result for other alloys was reported in previous reports [1, 7, 9, 16, 23, 25, 31].

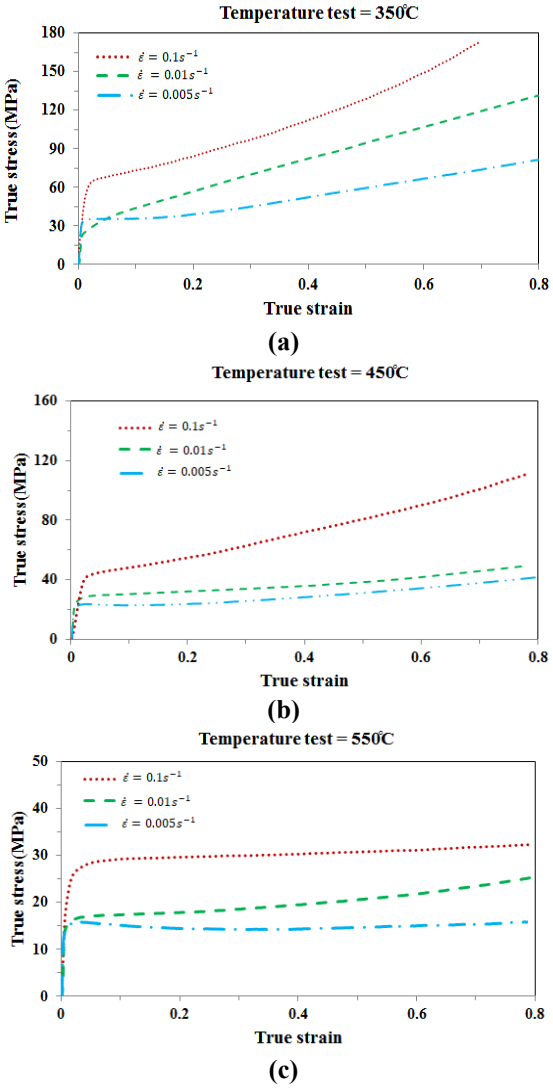

Fig. 6. True stress-true strain curves of AA6061T6-2 for various strain rates at different temperatures of (a) 350°C, (b) 450°C and (c) 550°C.

Owing to the high SFE of aluminum alloys, DRV is even more important to the softening process, In other words, DRV is a sufficient restoration mechanism at the high-temperature deformation of aluminum and a steady state of stress is reached. This is the result of the balance between hardening and softening mechanisms. The steady-state behavior depends on the Zener-Hollomon parameter. At the recovery stage, the dislocations of opposite sign annihilate each other by a combination of gliding and climbing mechanisms. The excess dislocations are left in the material at the end of the first stage of recovery. In materials with high SFE, the sub-grains or cell structure with low-angle grain boundaries (LAGBs) formed during deformation is gradually evolved into high-angle grain boundaries (HAGBs) due to efficient DRV with the migration of sub-grain boundaries, which is known as continuous dynamic recrystallization (CDRX) and occurs at the sufficiently high strain values [47-49].

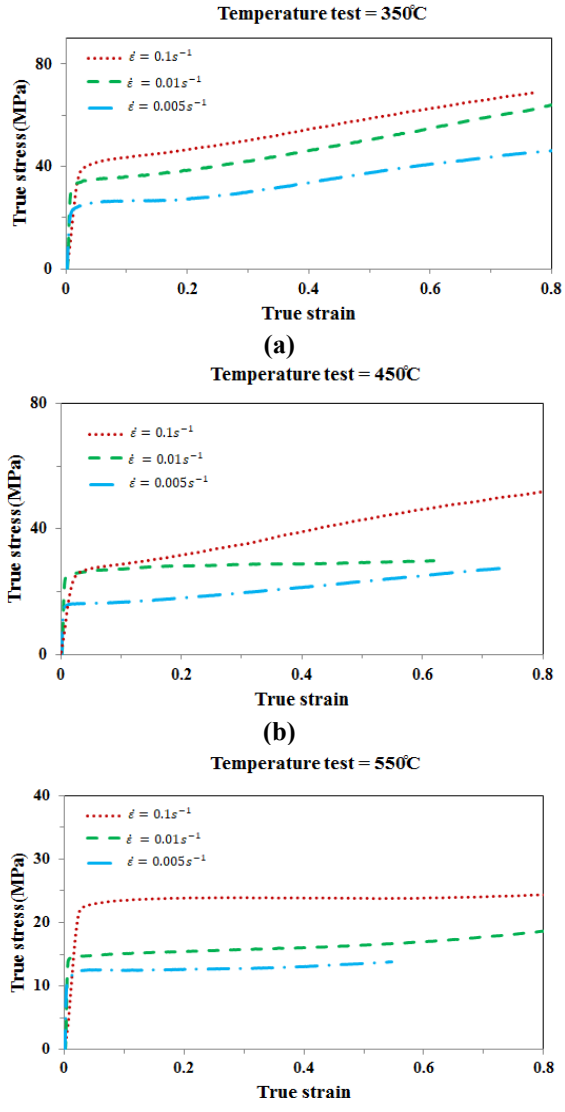

Fig. 7. True stress-true strain curves of AA6063T6-2 for various strain rates at different temperatures of (a) 350°C, (b) 450°C, and (c) 550°C.

[DOI: 10.22068/ijmse.1890]

The dominant recrystallization mechanism was assumed to be CDRX and experimental evidence was also shown. In CDRX, the progressive increase in the misorientation of the LAGB occurs due to sub-grain rotation or accumulation of dislocations along a sub-grain boundary. The progressive increase in the misorientation of the LAGBs gradually forms new HAGBs. When the steady-state is reached, a fully recrystallized microstructure is obtained [49]. In aluminum alloys, the occurrence of CDRX is attributed to the lowering of SFE caused by solute additions, particularly magnesium.

The true stress versus true strain curves obtained during the hot compression test under various strain rates and deformation temperatures for AA6063-T62 has been presented in Figure 7, as it is shown for AA6061 aluminum alloys. As it is clear, the strain effects on the flow stress are significant.

As temperature increases, both the stress and the difference between stresses decrease which is mainly associated with the precipitate distribution as reported by other researchers [6].

The flow stress at versus deformation temperatures and strain rates have been presented as a three-dimensional plot as shown in Figures 8 (a) and (b) for A6061 T6-2 and AA6063 T6-2 respectively, that confirm above-mentioned results. It presents that the influences of the strain rate and temperature on the flow stress are considerable. As the decrease in temperature and the increase of strain rate can increase flow stress. By increasing the strain rate, the strain is applied in less time so the opportunity for the occurrence of dynamic recovery in the material decreases due to decreased time for atomic diffusion and reduced probability of occurrence of diffusion phenomenon. However, at high strain rates, there is not enough time for the movement of the dislocations and to join together to form cell or sub-grain boundaries (and finally to create the cell sub-grains or structure). Therefore, as it has been reported by Mortezaei et al. [50], DRV is retarded and work hardening dominates at high value of strain rates. The evolution of the dislocation density depends on two simultaneous mechanisms: dislocation nucleation or generation and annihilation. At the high values of strain rates, the strain rate sensitivity (SRS) (m) declines correspondingly with the increase of the temperature at a strain of 0.8. It is observed that the true stress increases remarkably with the strain rate at the temperature of 350°C. However, when deformed at 550°C, the slope becomes moderate. This may be explained by the fact that the strengthening effects caused by strain rate hardening and strain hardening of the alloy are counteracted by the thermal softening within the strain rate considered in this study which was reported in the other researches [51, 52].

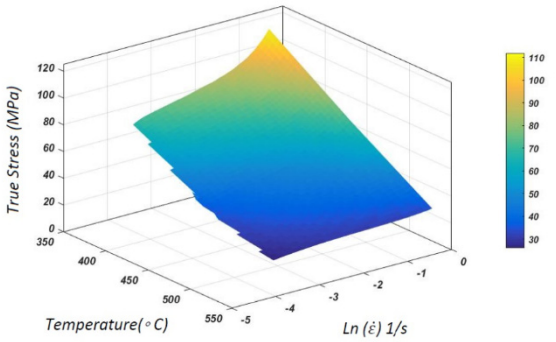

(a)

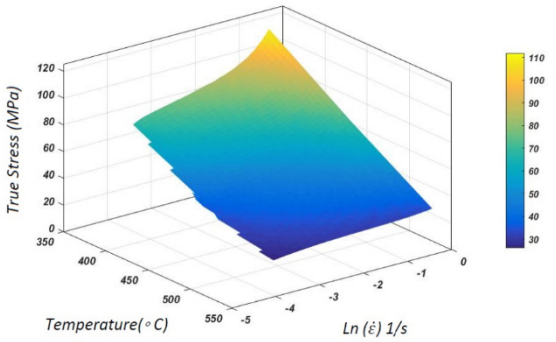

(b)

Fig. 8. Representation of flow stress as a function of temperature and strain rate at a strain of 0.8 for (a) AA6061T6-2 and (b) AA6063T6-2.

3.2. True stress-true strain curves of AA6061 and AA6063 with different heat treatments

As the decrease in temperature and the increase of strain rate can increase flow stress. Also, the strain effects on the flow stress are significant. Therefore, at the beginning deformation that the flow stress has low value, stress increases sharply with the increase of strain due to the significant work hardening effect. Figure 9 (a) to (c) show the true stress–the true strain of the AA6061 aluminum alloy treated with different heat treatment conditions at deformation temperatures of 350, 450, and 550°C respectively. The results present that the influences of the heat treatment conditions on the flow stress are considerable at

[DOI: 10.22068/ijmse.1890]

any deformation temperature. For both aluminum alloys which were heat-treated by age hardening (T6-1 and T6-2) and annealing (O), the flow stress decreased with an increase of temperature and a decrease of strain rate.

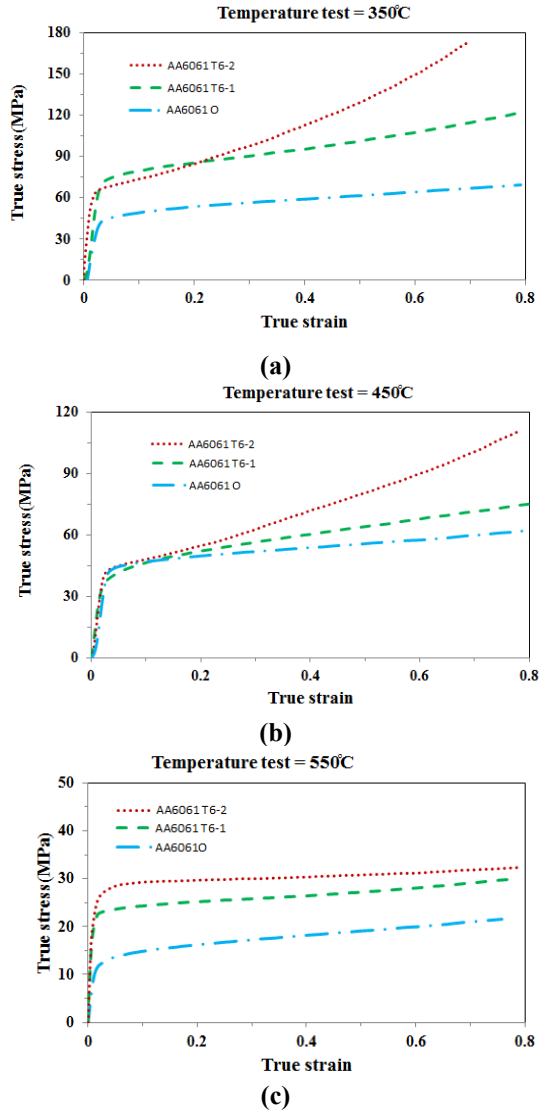

Fig. 9. True stress-true strain curve of AA6061 O, AA6061 T6-1, and AA6061 T6-2 during hot compression deformation at $\dot{\varepsilon}$ =0.1s^{-1} and different temperatures of (a) 350, (b) 450, and (c) 550°C.

Under all of the deformation temperatures of 350-550°C, the flow stresses of the alloy treated by the T6-1 and T6-2 age hardening (AA6061 T6-1 and AA6061 T6-2) were greater than that of the alloy treated by O annealing (AA6061 O) at all the strain rates investigated. As it is obvious in these curves, for different heat treatment conditions, the configuration of flow curves are different.

At the lower deformation temperatures of 350°C and 450°C, with increasing strain, for both the age-hardened AA6061 T6-1 and AA6061 T6-2 alloys and annealed AA6061 O alloy, the stress of each flow curve exhibits an initial rapid increase to stress values, as the flow stresses of AA6061 T6-2 have a significant increase in compared to other alloys and after that are the flow stresses of AA6061 T6-1 and AA6061 O alloys consequently, whereas with increasing deformation temperature to 550°C, as the strain increases each flow curve exhibits an initial rapid increase in stress to the indicated value, followed by a gradual increase in flow stress. For the annealed alloy, however, no significant flow increasing occurs under any of the deformation conditions.

Therefore, at the beginning deformation that the flow stress has low value, stress increases sharply with the increase of strain due to the significant work hardening effect as this effect will be more pronounced on the age-hardened precipitation alloys consist of AA6061 T6-1 and AA6061 T6-2. The results show that flow stress increases with increasing precipitations of aluminum alloy, so work hardening rate increases with increasing precipitations because it prevents dislocation movement and pins dislocations during forming at low deformation temperature values and increase the flow stress, whereas the dissolution of some of the precipitations occurs with increasing deformation temperature to 550°C. Similar behavior were reported by Zhang et al [42].

Figure 10 shows the microstructures of hot deformed AA6061 at a strain of 0.8 and different deformation temperature, strain rate, and heat treatment. It indicates that the precipitate values have decreased and grain refinement has occurred at the deformation temperature of 550°C rather than temperatures of 350°C and 450°C. Consequently, the reduction of precipitate values (equivalent to the reduction of volume fraction) consistent with the Zener dragging theory has a direct correlation with the drag force applied to the grain boundaries [53, 54]. In other words, fewer precipitates mean less drag force. As a result, due to the reduction of drag force, the flow stress at higher temperatures has also decreased. Also, a dynamic Zener pinning pressure can strongly suppress nucleation and/or retard recrystallization resulting in a sluggish

[DOI: 10.22068/ijmse.1890]

recrystallization reaction and an inhomogeneous grain structure of coarse elongated grains as has been reported by other researchers [55].

DRV has been shown to occur more strongly in high SFE metals and alloys consist of aluminum alloy. Therefore, CDRX is considered a dominant mechanism from sub-grain structures in hot deformation [27, 29]. The CDRX kinetics are slowed by Zener pinning via pinning of sub-grain structures and inhibition of nucleation and as clear in Figure 10 (d), the recrystallized grain size of the hot deformed precipitated AA6061T6-2 is larger than of the hot deformed AA6061 O aluminum alloy, as was reported by Humphreys et al. [40]

In low strain rate and low deformation temperature (0.01 s^{-1}, 350°C), the grains show up an elongated morphology revealing that work hardening and partial dynamic recovery as important typical characteristics occur (Figures 10(a) and (c)). In contrast, as clear in Figures 10 (b) and (d), some recrystallized grains are detected with increasing temperature to 550°C revealings that partial dynamic recrystallization has happened [6]. Figures 11 (a) to (c) show the true stress–the true strain of the AA6063 aluminum alloy treated with different heat treatment conditions at deformation temperatures of 350, 450, and 550°C, respectively. The results present that the influences of the heat treatment conditions on the flow stress are considerable at any deformation temperature. For both aluminum alloys which were heat-treated by age hardening (T6-1 and T6-2) and annealing (O), the flow stress decreased with an increase of temperature and a decrease of strain rate. Under all of the deformation temperatures of 350-550°C, the flow stresses of the alloy treated by the T6-1 and T6-2 age hardening (AA6063 T6-1 and AA6063 T6-2) were greater than that of the alloy treated by O annealing (AA6063 O) at all the strain rates investigated. As it is obvious in these curves, for different heat treatment conditions, the configuration of flow curves are different. At the lower deformation temperatures of 350 and 450°C, with increasing strain, for both the age-hardened AA6063 T6-2 and AA6063 T6-1 alloys and annealed AA6063 O alloy, the stress of each flow curve exhibits an initial rapid increase to stress values, as the flow stresses of AA6063 T6-2 have a significant increase in compared to other alloys and after that are the flow stresses of AA6063 T6-1 and AA6063 O alloys consequently, as it was seen for AA6061 aluminum alloy.

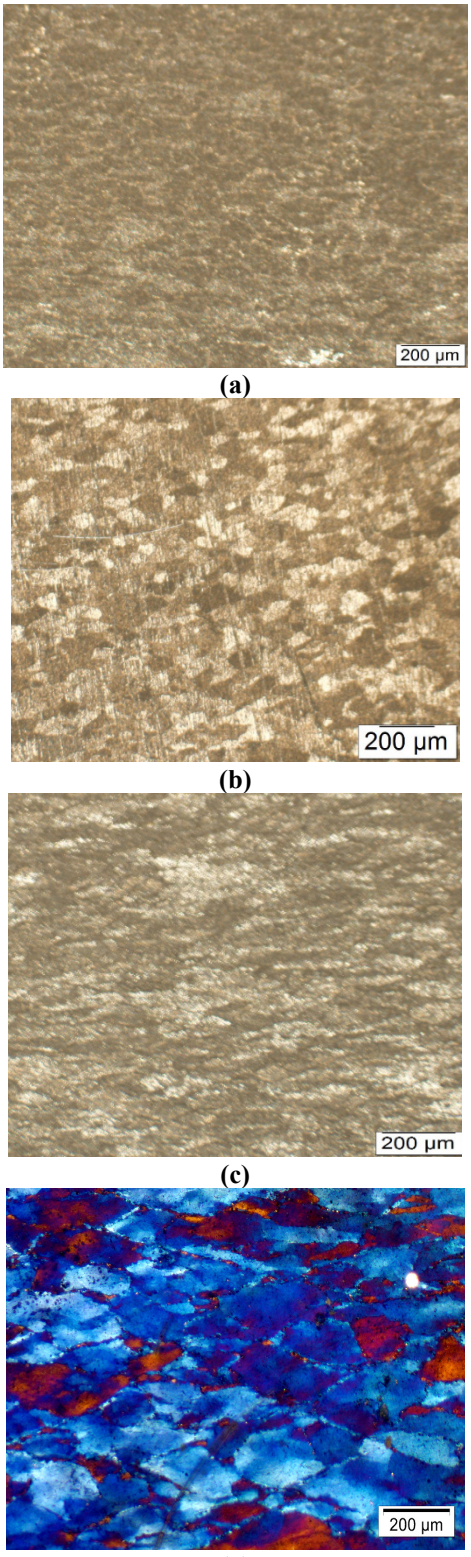

Fig. 10. Microstructures of the hot deformed AA6061 O at the center of the deformed samples and different processing parameters of (a) 350 °C and 0.01 s^{-1} and (b) 550°C and 0.005 s^{-1} and the hot deformed AA6061 T6-2 at different processing parameters of (c) 350 °C and 0.01 s^{-1} and (d) 550°C and 0.005 s^{-1}.

[DOI: 10.22068/ijmse.1890]

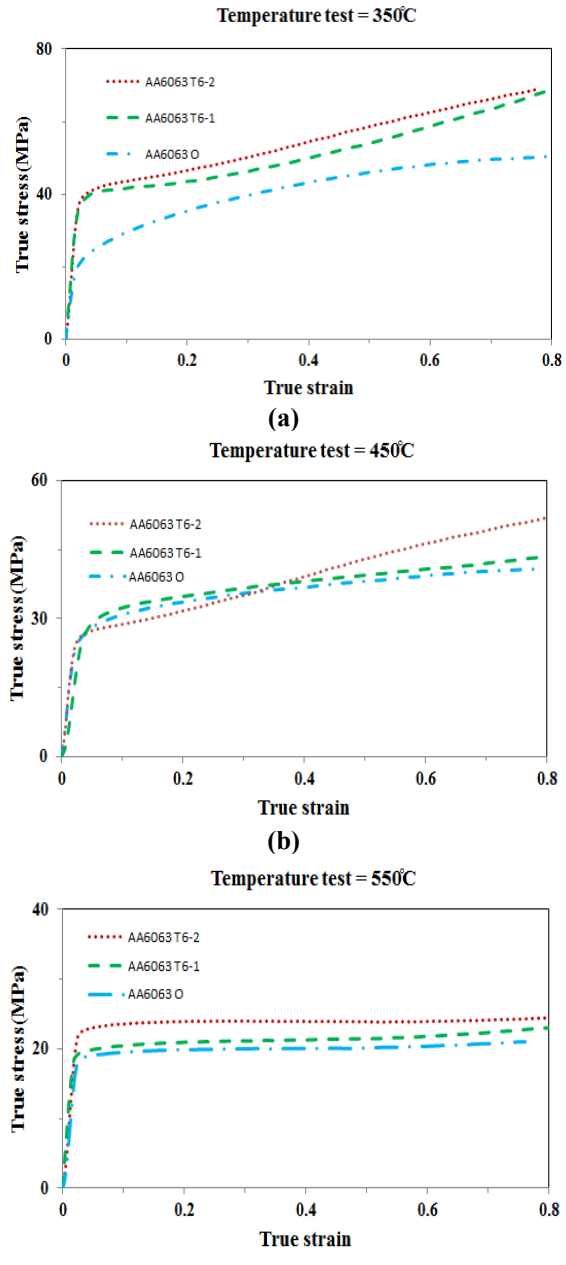

Fig. 11. True stress-true strain curves of AA6063 T6-2, AA6063 T6-1, and AA6063 O during hot deformation at $\dot{\varepsilon}$ =0.1$s^{-1}$and different temperatures of (a) 350, (b) 450, and (c) 550°C.

Whereas with increasing deformation temperature to 550°C, as the strain increases each flow curve exhibits an initial rapid increase in stress to indicated value, followed by a gradual steady-state in flow stress. Therefore, at the beginning deformation that the flow stress has low value, stress increases sharply with the increase of strain due to the significant work hardening effect as this effect will be more pronounced on the age-hardened precipitation alloys consist of AA6063 T6-1 and AA6063 T6-2. The results show that flow stress increases with increasing precipitations of aluminum alloy, so work hardening rate increases with increasing precipitations because it prevents dislocation movement and pins dislocations during forming at low deformation temperature values and increase the flow stress, whereas the dissolution of some of the precipitations occurs with increasing deformation temperature to 550°C. As it is clear in Figure 11(c), the difference in the flow stress values for different heat-treated AA6063 (T6-2, T6-1, and O) is very small at the deformation temperature of 550°C.

The activity of boundaries increased and the LAGBs (subgrains) gradually stabilized and transformed into HAGBs (equiaxed grains) under the subsequent hot forming (at a high temperature of 550°C and accumulated deformation 0.6) [37]. The activities of dislocations and sub and grain boundaries increase with increasing the deformation temperature and it is easier for their migration and merging and finally leading to more DRV, and more obvious grain refinement [57], indicating that precipitates can be re-dissolved during hot deformation at a higher value of deformation temperature from solution temperature (400-500°C) of aluminum alloy, However, the redissolution may be insufficient at high values of strain rates (higher than 0.1 s^{-1}).

Figures 12(a) and (b) show the microstructures of hot deformed AA6063 T6-2 and AA6063 O aluminum alloy at the center of the deformed sample, respectively, at a deformation temperature of 550°C and strain rate of 0.005 s^{-1}.

As it is clear, deformation at low temperatures leads to an increase in the dislocation density of the deformed specimen. Restoration mechanisms are activated and recrystallized grains are observed in the microstructures by increasing deformation temperature.

For more clarification, the comparative rectangular charts of flow stress at strain rate 0.1 are shown in Figure 13 and Figure 14 for AA6061 and AA6063 alloys, respectively. It is clear in these figures that the difference in flow stress between aged and annealed specimens decreases with increases in the deformation temperature for both investigated alloys, because of fewer precipitates in alloys matrix in higher deformation temperature. By comparing the flow stress of

[DOI: 10.22068/ijmse.1890]

T6-1 and T6-2, it can be described that T6-2 heat treatment has more effect on flow stress, and in the same condition flow stress of T6-2 samples is more than T6-1 samples.

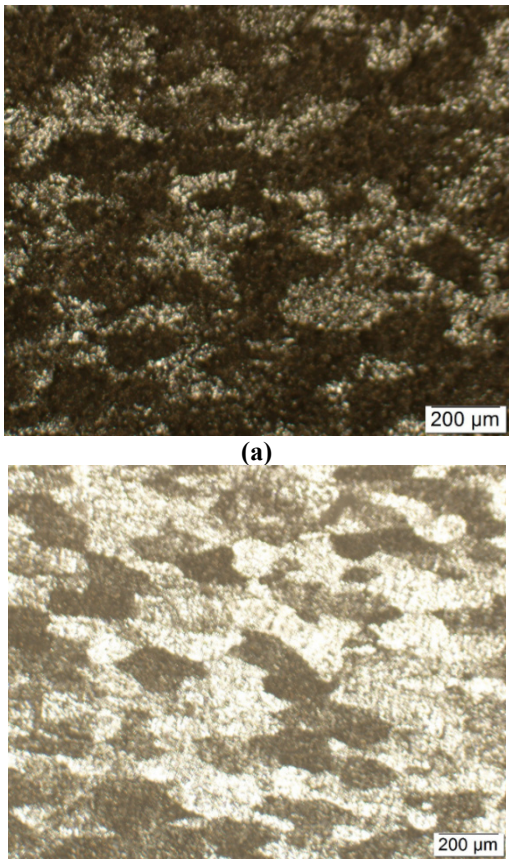

Fig. 12. Microstructures of hot deformed (a) AA6063 T6-2 and (b) AA6063 O alloys at deformation temperature of 550°C and strain rate of 0.005 s^{-1}.

It is clear from comparing Figure 13 and Figure 14 that the type of heat treatment has more effects on the mechanical behavior of AA6061 aluminum alloy compare to AA6063 aluminum alloy, and also the ranges of flow stress of all conditions of AA6061 are greater than AA6063.

As a result, the type of heat treatment of both alloys has a lesser effect at a higher temperature and lower strain rate test, on the other hand, the type of heat treatment has less effect on alloy behavior. Similar behavior were reported by other researchers [42].

Figure 15 and Figure 16 indicate these results for both alloys at a strain and strain rate of 0.55 and 0.005 s^{-1}, respectively. It can be a result of the dissolution of precipitation at higher temperatures as a similar result was reported by others [7, 56]. This result can be seen in Figure 17 for AA6061

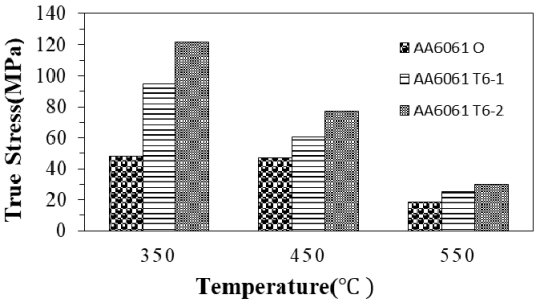

Fig. 13. The effects of heat treatment of AA6061 alloy on the flow stress at ε=0.5.

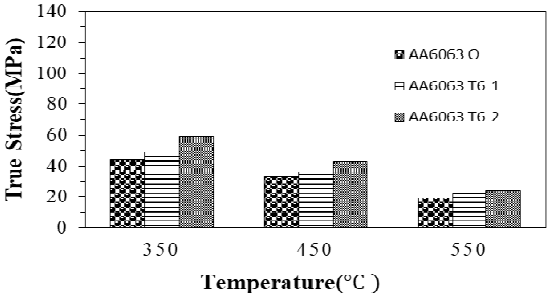

Fig. 14. The effects of heat treatment of AA6063 alloy on the flow stress at ε=0.5.

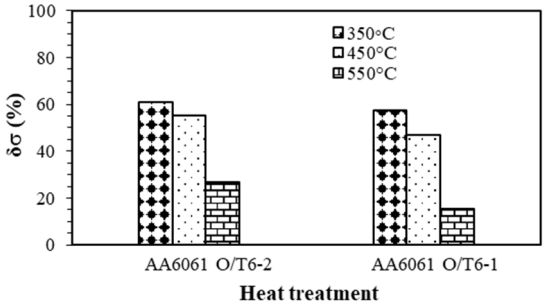

Fig. 15. The difference in flow stress between aged and annealed AA6061 alloys.

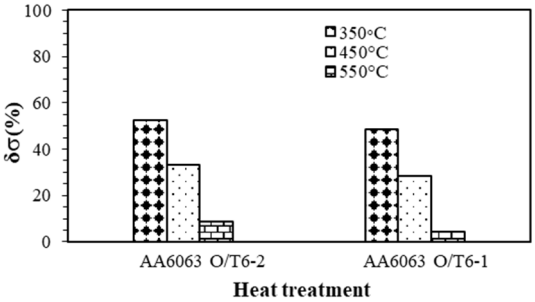

Fig. 16. The difference in flow stress between aged and annealed AA6061 alloys.

at a deformation temperature of 550°C. By comparing the microstructure of initial and deformed specimens in Figure 2 and Figure 17, respectively, it is clear that the precipitation decreases at high temperatures in comparison with low temperatures.

[DOI: 10.22068/ijmse.1890]

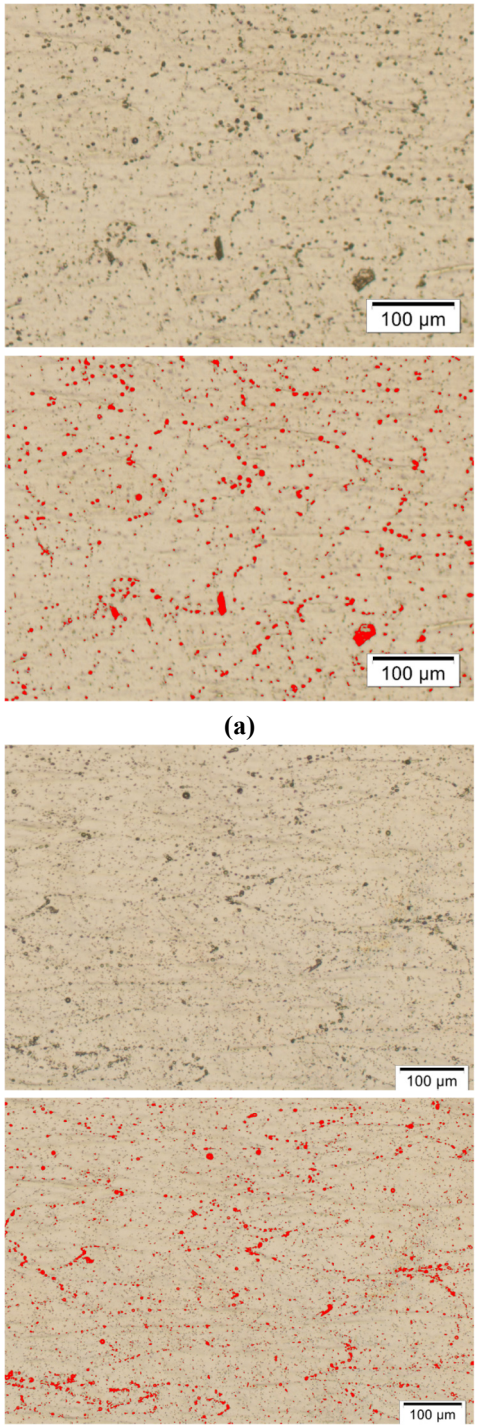

Fig. 17. Dissolution of precipitation in the deformed (a) AA6061 O and (b) AA6061 T6-2 alloys at deformation temperature of 550°C.

Plenty of spherical precipitates wrapped by dislocations were produced during the initial stage of deformation especially at low deformation temperature, in contrast, the mobility of dislocations reduced by these precipitates. With increasing deformation temperature, further recovery occurs and dislocation cells form and the activity of dislocations is increased while precipitates partially were dissolved, resulting in weakening of the pinning effects of precipitates. Dislocations become ordered and rearranged to form sub-grains [57]. Dislocations induced by deformation were entangled and recovered to form dislocation cells. The spheroidized Mg_2Si particles pinned dislocations and boundaries which led to the sub-grains formation during the hot deformation at a high value of deformation. The transformation of LAGBs into HAGBs could have been accelerated by the pinning effect of precipitates and accumulated deformation during further hot compression.

3.3. Hardening rate

In the plastic region of deformation, the derivative of the true stress with regard to the true strain yields the work hardening rate, θ [20]. In an isothermal condition, the slope of the stress versus plastic strain curve derived from a constant true strain rate test reflects the evolution of the internal variable [21]. The hardening rate value was achieved using the central difference approach [22] by the following equation:

$$\theta_i = \frac{d\sigma}{d\varepsilon}\Big|_i = \frac{\sigma|_{i+1} - \sigma|_{i-1}}{\varepsilon|_{i+1} - \varepsilon|_{i-1}} \quad (1)$$

Figures 18 (a) and (b) show the work hardening versus true stress for AA6061 alloy that treated by T6-1, T6-2, and O, at the strain rate of 0.1 s^{-1} and deformation temperature of 350°C and 550°C, respectively. Figures 19 (a) and (b) show the work hardening versus true stress for AA6063 alloy that treated by T6-1, T6-2 age hardening, and O annealing, at the strain rate of 0.1 s^{-1} and deformation temperature of 350°C and 550°C, respectively.

The primary steep slopes of the work-hardening rate curves relate to the early plastic deformation region of the material (As it is obvious in Figures 18 and 19). After passing the initial part of curves, the work hardening slope suddenly decreases to the second region. In this region, slopes of the work hardening rate curves gradually decrease by increasing either the plastic stress or strain and this inclination gets to zero or constant values due to the restoration mechanism which is mainly dynamic recovery [23] and dissolution of precipitation in the deformed age-hardened aluminum alloys.

[DOI: 10.22068/ijmse.1890]

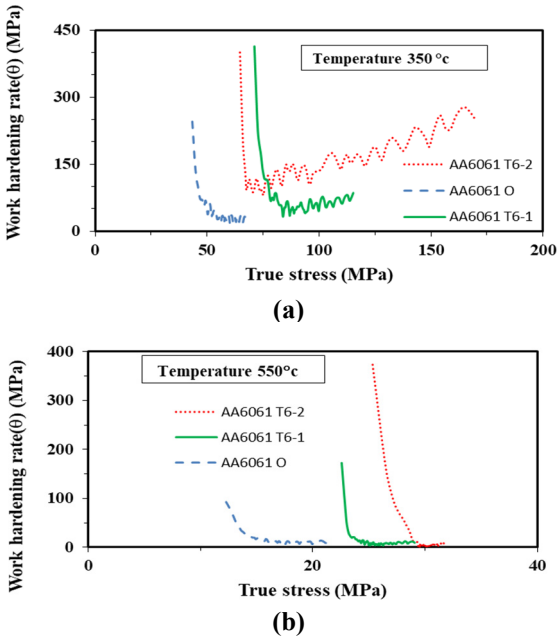

Fig. 18. Work hardening rate (θ) versus true stress for different heat-treated AA6061 alloys at deformation temperature of (a) 350 °C, and (b) 550 °C.

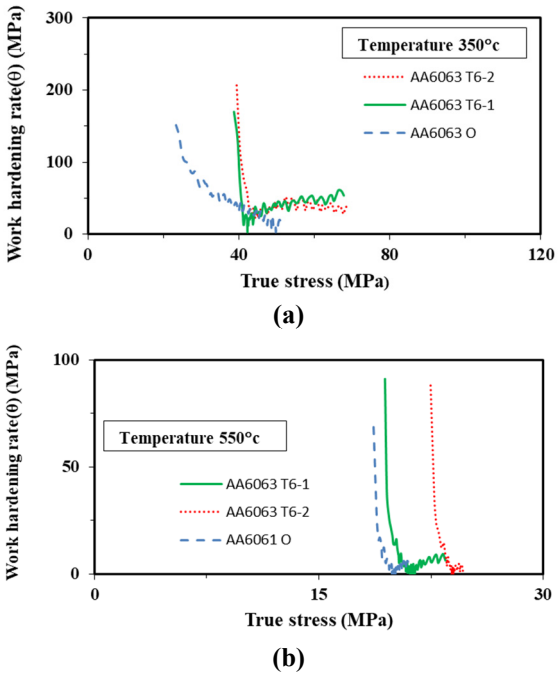

Fig. 19. Work hardening rate (θ) versus flow stress (σ) for AA6063 at deformation temperature of (a) 350°C, and (b) 550 °C.

In some conditions such as high deformation temperature and low strain rate, the hardening rates attain zero value (θ = 0), which corresponds to a balance between hardening processes and the restoration mechanism of dynamic recovery and dissolution of precipitation. These slopes variations show variation in the restoration and softening mechanisms. The variations of these curves with the variation of heat treatment illustrate the effects of annealing and aging heat treatment of aluminum alloys on the softening mechanism.

Stage I is the hardening condition which indicates the formation and accumulation of dislocations. Stage II is the location of the inflection point ($d\theta/d\sigma = 0$) in the curve, which indicates the critical conditions (ε_c and σ_c) for the onset of DRV and/or nucleation of recrystallization. Stage III is the development of the DRV mechanism in which the slope of the curve gradually decreases by an increase in strain. When the θ reaches zero at this step, it shows the peak strain and corresponding peak stress which represents the transient equilibrium between work hardening and work softening.

For both alloys, at a higher temperature, the range of hardening rate reduces, because the hardening rate is the slope of true stress versus plastic strain curve, and as mentioned stress range is found to decrease with increasing temperature. As is expected hardening rate is higher for T6-1 and T6-2 samples compared to annealed samples and the hardening rate differences of aged and annealed aluminum alloys (both AA6061 and AA6063 aluminum alloys) decrease with increasing deformation temperature to 550°C.

4. CONCLUSIONS

In this paper, the influence of aging and annealing heat treatment of AA6061and AA6063 aluminum alloy on the thermo-mechanical behavior was investigated by isothermal hot compression tests in various ranges of strain rates and temperatures. Based upon the results obtained, the following conclusions can be stated:

The flow stress is highly sensitive to deformation temperature and strain rate as it increases with increasing strain rate and decreasing deformation temperature.

The type of heat treatment has a significant influence on the mechanical behavior of AA6061 and AA6063 aluminum alloy at elevated deformation temperatures, and the effect is on the flow behavior of AA6061 aluminum alloy compare to AA6063 aluminum alloy.

For both alloys, the effects of heat treatment on

[DOI: 10.22068/ijmse.1890]

the thermo-mechanical behavior of aluminum alloys decrease with increase in deformation temperature as the type of heat treatment has less effect with increasing temperature.

Microstructural investigations of deformed specimens indicate that dislocation density increases and precipitates coarsen and the dissolved elements are deleted from the matrix at low deformation temperature. Whereas, annihilation and rearrangement of dislocations happen and the amount of solute elements in the matrix increases owning to the higher diffusion rate of dissolved elements. Therefore, the volume fraction of precipitations decreases with increasing deformation temperature from 350 to 550°C, continuously. The precipitation decreases at high temperatures in comparison to low temperatures

For both alloys, the work hardening rate is higher for aged (T6-1 and T6-2) samples compared to annealed (O) samples, and also the range and differences of hardening rate reduce at higher temperatures.

5. REFRENCES

[1] Ye. Tuo, L.L., Guo. Pengcheng, Xiao. Gang, Chen. Ziming, Effect of aging treatment on the microstructure and flow behavior of 6063 aluminum alloy compressed over a wide range of strain rate. International Journal of Impact Engineering, 2016. 90, 72-80.

[2] Badami, E., M. Salehi, and S. Seyedein, Modeling high temperature flow behavior of an al 6061 aluminium alloy. Iranian Journal of Materials science and engineering, 2014. 11(4), 63-71.

[3] Fan. Xiao-bo, H.Z.-b., Zhou. Wen-xuan, Yuan. Shi-jian, Formability and strengthening mechanism of solution treated Al–Mg–Si alloy sheet under hot stamping conditions. Journal of Materials Processing Technology, 2016. 228, 179-185.

[4] Mrówka-Nowotnik, G., Influence of chemical composition variation and heat treatment on microstructure and mechanical properties of 6xxx alloys. Archives of materials science and engineering, 2010. 46(2), 98-107.

[5] Swamy. NR Prabhu, R.C., Chandrashekar. T, Effect of heat treatment on strength and abrasive wear behaviour of Al6061-SiC p composites. Bulletin of Materials Science, 2010. 33(1), 49-54.

[6] Hawas, M.N., Effect of Ageing Time on Adhesive Wear of AL Alloy AA6061-T6. journal of kerbala university, 2013. 11(4), 145-152.

[7] Ezatpour. HR, S.M.H., Sajjadi. Seyed Abdolkarim, Huang. Yz, Investigation of work softening mechanisms and texture in a hot deformed 6061 aluminum alloy at high temperature. Materials Science and Engineering: A, 2014. 606, 240-247.

[8] Grajcar. A, O.M., Fojt-Dymara. G, The influence of hot-working conditions on a structure of high-manganese steel. Archives of Civil and Mechanical Engineering, 2009. 9(3), 49-58.

[9] Rezaei Ashtiani, H.R. and P. Shahsavari, Strain-dependent constitutive equations to predict high temperature flow behavior of AA2030 aluminum alloy. Mechanics of Materials, 2016. 100, 209-218.

[10] He, J., Chen, Fei, Wang, Bo, Zhu, Luo Bei, A modified Johnson-Cook model for 10% Cr steel at elevated temperatures and a wide range of strain rates. Materials Science and Engineering: A, 2018. 715, 1-9.

[11] Xu, L., Chen, Liang, Chen, Gaojin, Wang, Maoqiu, Hot deformation behavior and microstructure analysis of $25Cr_3Mo_3NiNb$ steel during hot compression tests. Vacuum, 2018. 147, 8-17.

[12] Li, H.-Y., Li, Yang-Hua, Wang, Xiao-Feng, Liu, Jiao-Jiao, Wu, Yue, A comparative study on modified Johnson Cook, modified Zerilli–Armstrong and Arrhenius-type constitutive models to

[DOI: 10.22068/ijmse.1890]

predict the hot deformation behavior in 28CrMnMoV steel. Materials & Design, 2013. 49, 493-501.

[13] Lin, Y., Li, Qi-Fei, Xia, Yu-Chi, Li, Lei-Ting, A phenomenological constitutive model for high temperature flow stress prediction of Al–Cu–Mg alloy. Materials Science and Engineering: A, 2012. 534, 654-662.

[14] Chen, X., Liao, Qiyu, Niu, Yanxia, Jia, Weitao, Le, Qichi, Cheng, Chunlong, Yu, Fuxiao, Cui, Jianzhong, A constitutive relation of AZ80 magnesium alloy during hot deformation based on Arrhenius and Johnson–Cook model. Journal of Materials Research and Technology, 2019. 8(2), 1859-1869.

[15] Bobbili, R., Madhu, Vemuri, Constitutive modeling of hot deformation behavior of high-strength armor steel. Journal of Materials Engineering and Performance, 2016. 25(5), 1829-1838.

[16] Rezaei Ashtiani, H.R., H. Bisadi, and M. Parsa, Influence of thermomechanical parameters on the hot deformation behavior of AA1070. Journal of Engineering Materials and Technology, 2014. 136(1).

[17] Rezaei Ashtiani, H.R. and P. Shahsavari, A comparative study on the phenomenological and artificial neural network models to predict hot deformation behavior of AlCuMgPb alloy. Journal of Alloys and Compounds, 2016. 687, 263-273.

[18] Rezaei Ashtiani, H.R., P. Shahsavari, Constitutive modeling of flow behavior of precipitation-hardened AA7022-T6 aluminum alloy at elevated temperature. Trans. Nonferrous Met. Soc. China, 2020. 30, 2927−2940.

[19] Li, K., Pan, Qinglin, Li, Ruishi, Liu, Shuhui, Huang, Zhiqi, He, Xin, Constitutive modeling of the hot deformation behavior in 6082 aluminum alloy. Journal of Materials Engineering and Performance, 2019. 28(2), 981-994.

[20] Liu, S., Pan, Qinglin, Li, Hang, Huang, Zhiqi, Li, Kuo, He, Xin, Li, Xinyu, Characterization of hot deformation behavior and constitutive modeling of Al–Mg–Si–Mn–Cr alloy. Journal of Materials Science, 2019. 54(5), 4366-4383.

[21] Mostafaei, M., Kazeminezhad, Mohsen, Hot deformation behavior of hot extruded Al–6Mg alloy. Materials Science and Engineering: A, 2012. 535, 216-221.

[22] Nayak, K.C. and P.P. Date, Development of Constitutive Relationship for Thermomechanical Processing of Al-SiC Composite Eliminating Deformation Heating. Journal of Materials Engineering and Performance, 2019. 28(9), 5323-5343.

[23] Li, W., Li, Hai, Wang, Zhixiu, Zheng, Ziqiao, Constitutive equations for high temperature flow stress prediction of Al–14Cu–7Ce alloy. Materials Science and Engineering: A, 2011. 528(12), 4098-4103.

[24] McQueen, H., E. Fry, and J. Belling, Comparative constitutive constants for hot working of Al-4.4 Mg-0.7 Mn (AA5083). Journal of Materials Engineering and Performance, 2001. 10(2), 164-172.

[25] Cavaliere, P., E. Cerri, and E. Evangelista, Isothermal forging of AA2618+ 20% Al_2O_3 by means of hot torsion and hot compression tests. Materials Science and Engineering: A, 2004. 387, 857-861.

[26] Brown, S.B., K.H. Kim, and L. Anand, An internal variable constitutive model for hot working of metals. International journal of plasticity, 1989. 5(2), 95-130.

[27] Azarbarmas, M., Modeling the Dynamic Recrystallization by Using

[DOI: 10.22068/ijmse.1890]

Cellular Automaton: The Current Status, Challenges and Future Prospects, a Review. Iranian Journal of Materials Science and Engineering: 2020, 17 (4), 103-129.

[28] Guan, W., Linyuan, Kou, Zhiwen, Liu, Shikang, Li, Luoxing, Li, Flow softening behavior and microstructure evolution of aluminum alloy 6061 due to dynamic recovery. Materials Research Express, 2019. 6(5), 056555.

[29] Asgharzadeh, H., A. Simchi, and H. Kim, Dynamic restoration and microstructural evolution during hot deformation of a P/M Al6063 alloy. Materials Science and Engineering: A, 2012. 542, 56-63.

[30] Khodabakhshi, F., Simchi, A, Kokabi, AH, Gerlich, AP, Nosko, M, Effects of stored strain energy on restoration mechanisms and texture components in an aluminum–magnesium alloy prepared by friction stir processing. Materials Science and Engineering: A, 2015. 642, 204-214.

[31] Wei, C., GUAN, Ying-ping, WANG, Zhen-hua, Hot deformation behavior of high Ti 6061 Al alloy. Transactions of Nonferrous Metals Society of China, 2016. 26(2), 369-377.

[32] Chen, S., Chen, Kanghua, Peng, Guosheng, Chen, Xuehai, Ceng, Qinghua, Effect of heat treatment on hot deformation behavior and microstructure evolution of 7085 aluminum alloy. Journal of Alloys and Compounds, 2012. 537, 338-345.

[33] Jin, N., Zhang, Hui, Han, Yi, Wu, Wenxiang, Chen, Jianghua, Hot deformation behavior of 7150 aluminum alloy during compression at elevated temperature. Materials Characterization, 2009. 60(6), 530-536.

[34] Serajzadeh, S., Ranjbar Motlagh, S., Mirbagheri, S. M. H., Akhgar, J. M., Deformation behavior of AA2017–SiCp in warm and hot deformation regions. Materials & Design, 2015. 67, 318-323.

[35] Humphreys, F., The nucleation of recrystallization at second phase particles in deformed aluminium. Acta Metallurgica, 1977. 25(11), 1323-1344.

[36] Doherty, R., Hughes, DA, Humphreys, FJ, Jonas, J Juul, Jensen, D Juul, Kassner, ME, King, WE, McNelley, TR, McQueen, HJ, Rollett, AD, Current issues in recrystallization: a review. Materials Science and Engineering: A, 1997. 238(2), 219-274.

[37] Humphreys, F., Particle stimulated nucleation of recrystallization at silica particles in nickel. Scripta materialia, 2000. 43(7), 591-596.

[38] Daaland, O. and E. Nes, Recrystallization texture development in commercial Al1 Mn1 Mg alloys. Acta Materialia, 1996. 44(4), 1413-1435.

[39] Nes, E., N. Ryum, and O. Hunderi, On the Zener drag. Acta Metallurgica, 1985. 33(1), 11-22.

[40] Humphreys, F.J. and M. Hatherly, Recrystallization and related annealing phenomena. 2012, Elsevier.

[41] Eivani, A., J. Zhou, and J. Duszczyk, Grain boundary versus particle stimulated nucleation in hot deformed Al–4· 5Zn–1Mg alloy. Materials Science and Technology, 2013. 29(5), 517-528.

[42] Zhang, B., Baker, TN, Effect of the heat treatment on the hot deformation behaviour of AA6082 alloy. Journal of Materials Processing Technology, 2004. 153, 881-885.

[43] Ramachandran, T. Advances in Aluminium Processing and Its Automotive Application. in Workshop Lecture Notes. 2006.

[44] Esmaeili, S., Lloyd, DJ, Modeling of precipitation hardening in pre-aged AlMgSi (Cu) alloys. Acta materialia, 2005. 53(20), 5257-5271.

[DOI: 10.22068/ijmse.1890]

[45] Mukhopadhyay, P., Alloy designation, processing, and use of AA6XXX series aluminium alloys. ISRN Metallurgy, 2012.
[46] Kumar, R.V., Keshavamurthy, R, Perugu, Chandra S, Siddaraju, C, Influence of heat treatment on microstructure and mechanical behaviour of hot-rolled Al-Mg-Si alloy. Advances in Materials and Processing Technologies, 2020, 1-10.
[47] Jata, K., Semiatin, SLa, Continuous dynamic recrystallization during friction stir welding of high strength aluminum alloys. Scripta materiala, 2000. 43 (8), 743-749.
[48] Chen, H., Song, Bo, Guo, Ning, Liu, Tingting, Zhou, Tao, He, Jiejun, Dynamic Recrystallization and Grain Refinement in Extruded AZ31 Rod During Hot Torsion Deformation at 150°C. Metals and Materials International, 2019. 25(1), 147-158.
[49] Buzolin, R., Krumphals, F, Lasnik, M, Krumphals, A, Poletti, MC. A continuous dynamic recrystallization model to describe the hot deformation behaviour of a Ti5553 alloy. in Journal of Physics: Conference Series. 2019. IOP Publishing.
[50] Mortezaei, S., Arabi, H, Seyedein, H, Momeny, A, Soltanalinezhad, M, Investigation on Microstructure Evolution of a Semi-Austenitic Stainless Steel Through Hot Deformation. Iranian Journal of Materials Science and Engineering, 2020. 17(3), 60-69.
[51] Lee, W.-S., Sue, Wu-Chung, Lin, Chi-Feng, Wu, Chin-Jyi, The strain rate and temperature dependence of the dynamic impact properties of 7075 aluminum alloy. Journal of Materials Processing Technology, 2000. 100(1-3), 116-122.
[52] Ye, T., Wu, Yuanzhi, Liu, Wei, Deng, Bin, Liu, Anmin, Li, Luoxing, Dynamic Mechanical Behavior and Microstructure Evolution of an Extruded 6013-T4 Alloy at Elevated Temperatures. Metals, 2019. 9(6), 629.
[53] Yao, X., Zhang, Z, Zheng, YF, Kong, C, Quadir, Md Zakaria, Liang, JM, Chen, YH, Munroe, P, Zhang, DL, Effects of SiC nanoparticle content on the microstructure and tensile mechanical properties of ultrafine grained AA6063-SiCnp nanocomposites fabricated by powder metallurgy. Journal of materials science & technology, 2017. 33(9), 1023-1030.
[54] Du, L., Yang, Shaomei, Zhang, Peng, Du, Huiling, Pinning effect of different shape second-phase particles on grain growth in polycrystalline: numerical and analytical investigations. Composite Interfaces, 2018. 25(4), 357-368.
[55] Wang, N., Huang, Ke, Li, Yanjun, Marthinsen, Knut, The influence of processing conditions on microchemistry and the softening behavior of cold rolled Al-Mn-Fe-Si alloys. Metals, 2016. 6(3), 61.
[56] Fan, X., Li, M, Li, DY, Shao, YC, Zhang, SR, Peng, YH, Dynamic recrystallisation and dynamic precipitation in AA6061 aluminium alloy during hot deformation. Materials Science and Technology, 2014. 30(11), 1263-1272.
[57] Zuo, J., Hou, Longgang, Shu, Xuedao, Peng, Wenfei, Yin, Anmin, Zhang, Jishan, Effect of Deformation on Precipitation and the Microstructure Evolution during Multistep Thermomechanical Processing of Al-Zn-Mg-Cu Alloy. Metals, 2020. 10(11), 1409.

[DOI: 10.22068/ijmse.1890]